Transport Controlled Pattern Photopolymerization in a Single-Component System

Scott Meng,[†] Kumar Nanjundiah,[†] Thein Kyu,*[,†] Lalgudi V. Natarajan,[‡] Vincent P. Tondiglia,[‡] and Timothy J. Bunning[§]

Department of Polymer Engineering, University of Akron, Akron, Ohio 44325; Science Applications International Corporation, Dayton, Ohio 45431; and Air Force Research Laboratory, Materials and Manufacturing Directorate, Wright-Patterson Air Force Base, Ohio 45433

Received October 24, 2003; Revised Manuscript Received February 17, 2004

ABSTRACT: The purpose of the present paper is to extend the concept of pattern photopolymerization-induced phase separation of a binary blend to a single-component system containing pure photoreactive monomers with a minute level of photoinitiators. The patterning formation process was simulated in the framework of Cahn−Hilliard equation coupled with the photoreaction kinetic equation. Unlike binary systems undergoing photopolymerization-induced phase separation driven by thermodynamic force, the mechanism of pattern formation in the single-component system is essentially a photoreaction-induced transport phenomenon. Of particular interest is the observation of polymer concentration profiles evolving from a sinusoidal wave to various truncated ones. On the basis of two-wave interference optics, the microchannel layers have been fabricated. Resultant morphology was characterized using optical and atomic force microscopes. A two-dimensional light scattering device was utilized to study the diffraction patterns from the fabricated microchannel layers. The observed concentration profiles were compared with the theoretical predictions, and good agreement was found.

Introduction

In recent years, research on photopolymerization-induced phase separation in liquid crystal/polymer mixtures has attracted immense attention, especially in the fabrication of holographic polymer-dispersed liquid crystal (H-PDLC) with potential electrooptical applications[1−4] such as optical switches, information storage media, and microlens, among others. A typical methodology is to irradiate interfering laser beams over the photoreactive monomer/liquid crystal mixtures in the homogeneous state, triggering phase separation by pattern photopolymerization. The photopatterning technique operates on the principle of optical wave interference created by the constructive and destructive interference of two vertical waves and/or two horizontal waves, which produces regulated microchannel layers and/or microdroplet arrays. The mechanism governing photopolymerization-induced phase separation in a binary system has been vigorously investigated by several research groups.[5−7] Recently, pattern photopolymerization has been extended to preparing microporous films.[8,9] This approach is similar to that of H-PDLC mentioned above except that solvent replaces liquid crystals, which is subsequently extracted after the photopolymerization.

All of the aforementioned holographic methods generally involve a binary mixture as a starting material for the photopatterning.[10,11] In this paper, we have attempted to generate the microchannel layer patterns in a single-component system similar to those formed by photopolymerization in the binary blends. It is proposed to model the system in the framework of Cahn−Hilliard theory[12] coupled with a photopolymerization kinetic equation.

When light is irradiated on the sample by patterning via constructive and destructive interference of multiwaves, monomers are selectively polymerized in the high-intensity region of irradiation, whereas in the low-intensity region little or no reaction takes place. This creates a spatial concentration variation in the monomer field. Polymer chains, once formed, cannot diffuse away because of the chemical cross-links, although these molecules may undergo Brownian motion between the chemical junctions. Monomers are the ones that can transport through the polymer network. Strictly speaking, there may be some solubilizing agents and/or surfactant, though diminutive in amount, diffusing from high-intensity regions to low-intensity regions to fill the vacancy left by the monomers, and vice versa. In principle, the transport of monomers creates the polymer concentration contrast between the high-intensity region and the low-intensity region.

In the present paper, dynamics of photopolymerization-induced patterning in a single-component system is investigated, which is presumably governed exclusively by transport rather than thermodynamics. Other effects such as swelling of the network[10] and dimensional shrinkage[11] are not covered in this work, but it is not to say that those effects are not important to the dynamics studies and certainly deserves critical evaluation in the future.

Theoretical Scheme

The pattern forming aspects in a single-component system initiated by photopolymerization have been described through examination of the spatiotemporal development of the concentration order parameter of the monomer and/or polymer in the framework of the Cahn−Hilliard equation,[12] alternatively known as the time-dependent Ginzburg−Landau equation (TDGL model B),[13] which is coupled with a photopolymerization reaction kinetic equation. The Cahn−Hilliard equation

[†] University of Akron.
[‡] Science Applications International Corporation.
[§] Air Force Research Laboratory.
* Corresponding author: e-mail tkyu@uakron.edu.

10.1021/ma0356055 CCC: $27.50
Published on Web 04/20/2004

basically represents a spatiotemporal evolution of concentration order parameter, which may be expressed as

$$\frac{\partial \phi_m(r,t)}{\partial t} = \nabla\left[\Lambda_m \nabla\left(\frac{\delta G}{\delta \phi_m}\right)\right] + \eta_m \quad (1)$$

In eq 1, $\phi_m(r,t)$ is the conserved concentration order parameter of monomer at position r and time t. Furthermore, L_m represents the diffusivity of monomer. h_m represents the thermal noise in the monomer concentration field that satisfies the fluctuation−dissipation theorem.[14] In the simulation, the noise term was used only once in the first iteration, and it was removed in subsequent runs.

In the description of the temporal evolution of the compositional order parameter, the global free energy of the system may be written as

$$G = \int [g(\phi_m) + \kappa_m |\nabla \phi_m|^2]\, dV \quad (2)$$

where $g(\phi_m)$ is the local free density of the system. The $\kappa_m|\nabla\phi_m|^2$ in eq 2 is the nonlocal interfacial gradient term in which κ_m is the coefficient of interfacial gradient.[15] The local free energy density is of the usual Landau type:[16]

$$g(\phi_m) = \frac{r}{2}\phi_m{}^2 + \frac{u}{4}\phi_m{}^4 \quad (3)$$

where r and u are the coefficients of Landau-type free energy. For the single-component system, the sign of r should be positive which gives a single well. Alternatively, the fourth-order term may be omitted, and setting $r = 1$, a single well potential may be obtained. Inserting eqs 2 and 3 into eq 1 with some mathematical deductions and neglecting the interface term of eq 2 gives the classical equation that is known as Fick's second law of diffusion,[17] i.e.

$$\frac{\partial \phi_m(r,t)}{\partial t} = \nabla[\Lambda_m \nabla \phi_m] = D_m \frac{\partial^2 \phi_m}{\partial x^2} \quad (4)$$

where Λ_m can be simplified to the self-diffusion coefficient of monomer, D_m for the single-component system. It may be concluded that the Fick's diffusion equation is a special case of the Cahn−Hilliard equation.

The photopolymerization reaction kinetics may be expressed in the context of the first-order kinetic equation.[18] In the case of pattern irradiation, the light intensity varies periodically due to the constructive and destructive interference;[6,18] thus, the resulting reaction rate leads to

$$\frac{d\alpha}{dt} = k\left[1 + v\cos\left(\frac{2N_x\pi}{L}x\right)\right](1-\alpha) \quad (5)$$

where α is the conversion of the monomer and k is the overall reaction constant defined as $k = k_p(I_a/k_t)^{1/2}$ in which k_p and k_t represent the rate constants for propagation and termination of photopolymerization with I_a being the absorbed light intensity.[19] Here v symbolizes the visibility factor which controls the amplitude of the sinusoidal waves for incident light. N_x represents the number of layers associated with the periodicity in the vertical direction. L is the length of the assumed square grid.

Coupling eq 4 and eq 5, one obtains the classical reaction−diffusion equation:

$$\frac{\partial \phi_m(r,t)}{\partial t} = D_m \frac{\partial^2 \phi_m}{\partial x^2} - \alpha t \quad (6)$$

Note that eq 6 has been extensively employed elsewhere in modeling hologram formation,[20,21] which according to our derivations is just a special case of the generalized TDGL or the Cahn−Hilliard approach.

The spatiotemporal growth of the morphology has been simulated numerically based on the 256 × 256 grid using a finite central difference method for the spatial step and explicit forward difference method for the time step under periodic boundary conditions. Different grid sizes and time steps have been utilized to ensure the stability of the simulation. The reference system considered here is a single-phase multifunctional photocurable monomer.

Experimental Section

The monomer component used in the experiments is a commercially available epoxy acrylate SR-602 from Sartomer Inc. The photoinitiator, Rose Bengal derivatives, was received from Spectra group Ltd, Inc. The coinitiator *N*-phenylglycine (NPG), solubilizing agent, and surfactant such as octanoic acid were all purchased from Aldrich. The chemical structures of the components used in preparing the syrup are given in Figure 1. All the modifiers were used as received without further purification.

The syrup was mixed homogeneously for 24 h and then coated on a glass slide. The amounts of the photoinitiator, coinitiator, solubilizing agent, and surfactant are so small relative to the reactive monomer (SR-602) that the mixed syrup is transparent, suggestive of a single-phase character.

An illustration of the experimental holographic optical appartus for the two-wave interference is depicted in Figure 2, which consists of a green laser (wavelength of 532 nm, operated at 19 mW), beam splitters, spatial filters, plano-convex lens, mirrors, etc., in the optical trains. The pattern photopolymerization was realized through interference of the split coherent laser beams, giving a fringe width of 1−3 μm. The laser intensity at the sample was approximately 10 mW/cm^2, and the exposure time was 10 min unless indicated otherwise. Once the pattern photopolymerization was accomplished, morphological characterization was performed using the optical microscope (OM) from Nikon Corp. (model Optiphot-2) and the atomic force microscope (AFM) from Quesant Instrument Corp. (model Q-Scope 250) for surface topology investigations. The patterned samples were placed under a two-dimensional (2-D) light scattering device for diffraction patterns (see Figure 3). In the 2-D light scattering device, a 5 mW solid-state laser source (Power Technology) with a wavelength of 635 nm was employed together with a CCD detector (Apogee) to detect two-dimensional scattering images using the data acquisition, analysis, and control software from Sandoway Technology.

Results and Discussion

In Figure 4, (A) exhibits the optical micrograph of the photopatterned SR 602, displaying the microchannel layers under 2 min radiation. The bright region corresponds to the high-intensity area, which is rich in polymer, while the dark region is analogous to the low-intensity area where polymer is lean. As evident, each layer is formed with a high regularity. Subsequently, the surface topology of the microchannel layer patterns

A.

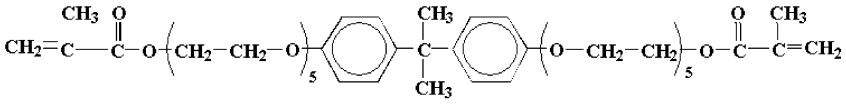

B.

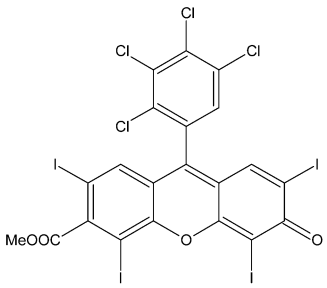

C.

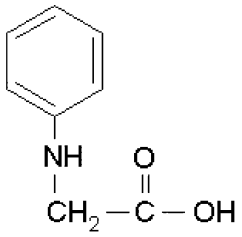

D.

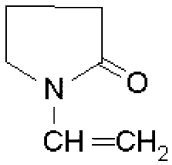

E.

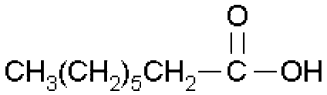

Figure 1. Chemical structures of monomer (SR-602) (A); photoinitiator, a Rose Bengal derivative (B); the coinitiator *N*-phenylglycine (NPG) (C); the solubilizing agent *N*-vinylpyrrolidone (NVP) (D); the surfactant octanoic acid (E).

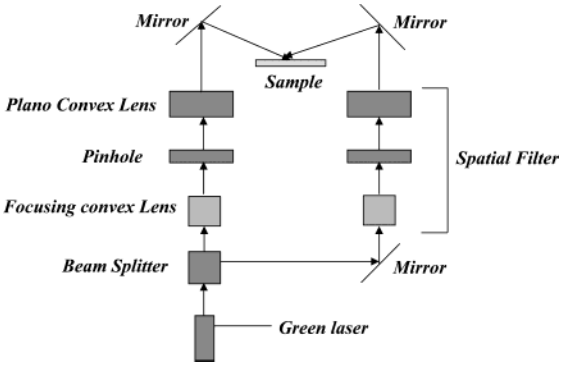

Figure 2. Illustration of two-wave interference experimental device.

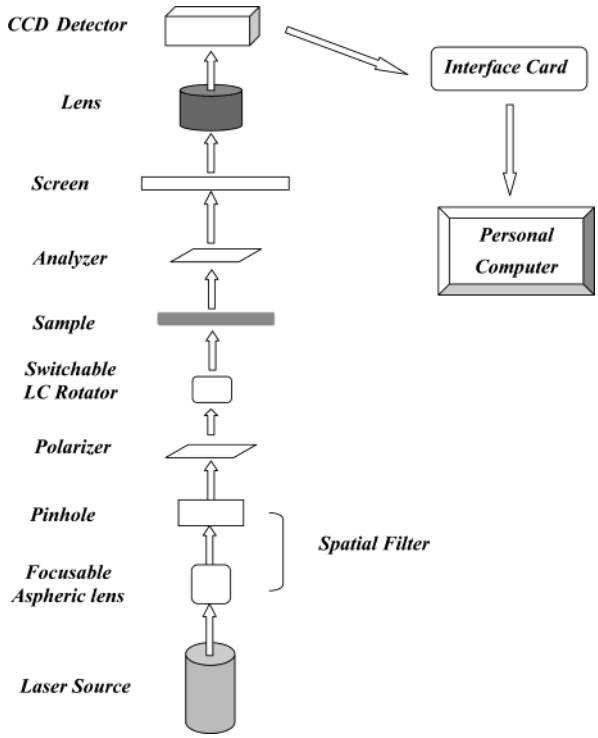

Figure 3. Demonstration of 2-D light scattering device.

of the same sample was further investigated by means of AFM using the height mode as depicted in Figure 4C. A clear contrast in the differential height can be discerned between the peak corresponding to the high-intensity region and the valley at the low-intensity region, thereby confirming the formation of microchannel layers seen under the optical microscope. It is apparent that the peaks consist of the emerging polymers, whereas the monomers predominantly reside in the valley. Further analysis of the horizontal slice of the microchannel layers reveals a sinusoidal profile as shown in Figure 4E. The amplitude of the undulation of the emerging polymers and the unreacted monomer regions is 60 nm in average.

Parts B, D, and F of Figure 4 are the respective microchannel layers graphs formed via 6 min radiation under the optical microscope, AFM, and height scan from AFM. No significant difference between the 2 min sample and the 6 min sample was observed at the first glance. For the purpose of confirmation, a number of experiments with 6 min radiation were undertaken and characterized by AFM. Parts G and H of Figure 4 are the consequent height scan profiles which are unlike what was seen in Figure 4F, displaying a deviation from sinusoidal such as a truncated flat-top or a crater. Although the diverse surface profiles are very intriguing, it should be cautioned that surface topology of the resultant gratings may not be free from artifacts such

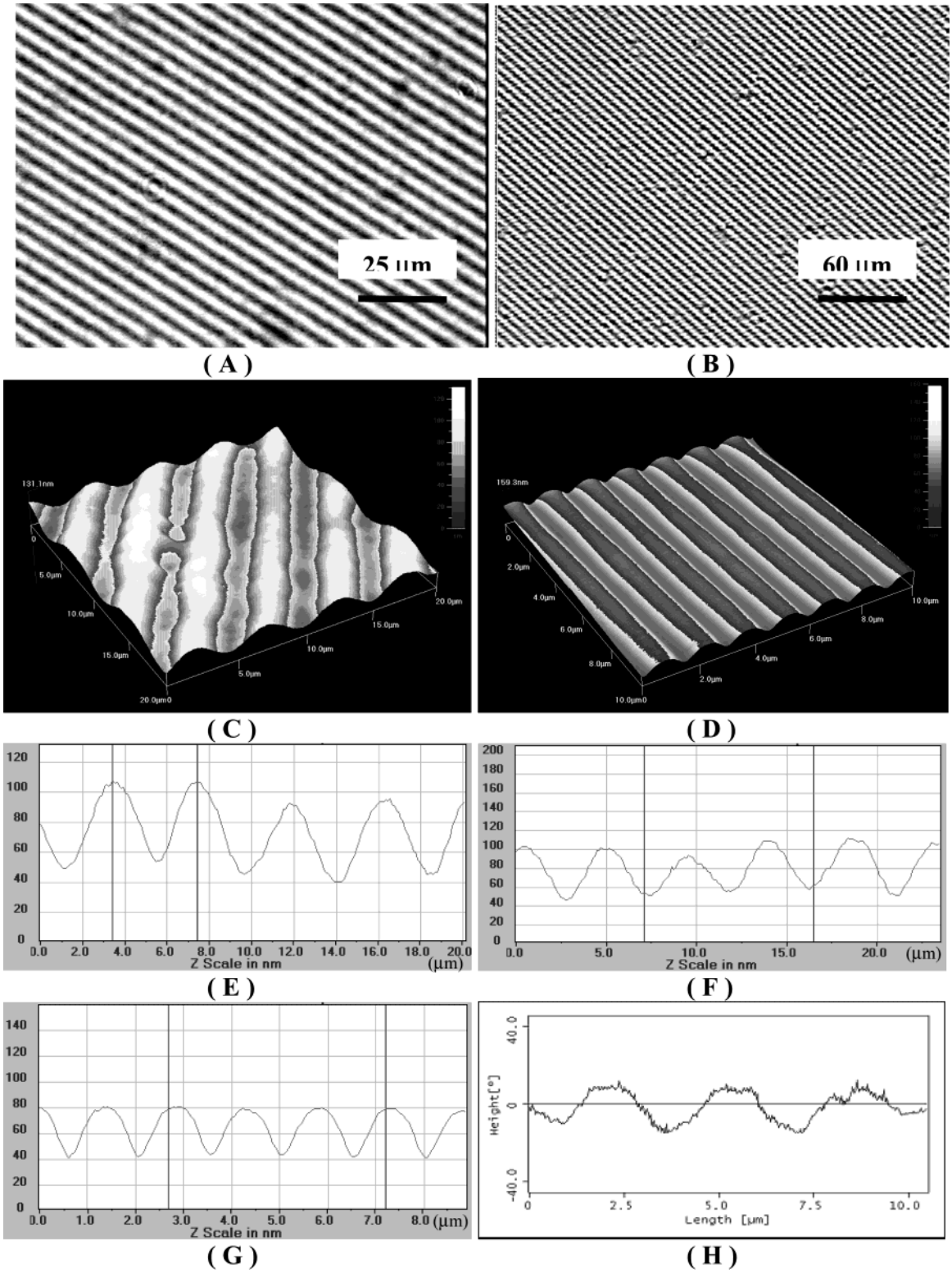

Figure 4. Experimentally fabricated microchannel layer pattern under 2 min radiation (A, C, E) and 6 min radiation (B, D, F) observed by an optical microscope (first row) and by an atomic force microscope (second row) and the height scan (third row) and other height scans showing cosine-square (G) and truncated surface profiles (H).

as surface tension at the polymer−air interface and wetting at the template. Most of all, surface topology is very likely to be different from the bulk concentration profiles throughout the sample thickness. It is therefore crucial to characterize the bulk concentration profile in reciprocal space using light scattering which gives the average overall scattering volume representing the bulk properties. Another important feature is that light scattering is capable of distinguishing the diffraction spots of the emerging sinusoidal structure (a single peak) from that of the nonsinusoidal profiles (multiple peaks).

The left graph in Figure 5 represents the diffraction pattern of the sample photocured for 2 min radiation using 2-D light scattering. A single diffraction peak was discerned on each side of the main beam, indicating the system bulk profile should be sinusoidal. The graph on the right was from the sample cured for 6 min radiation,

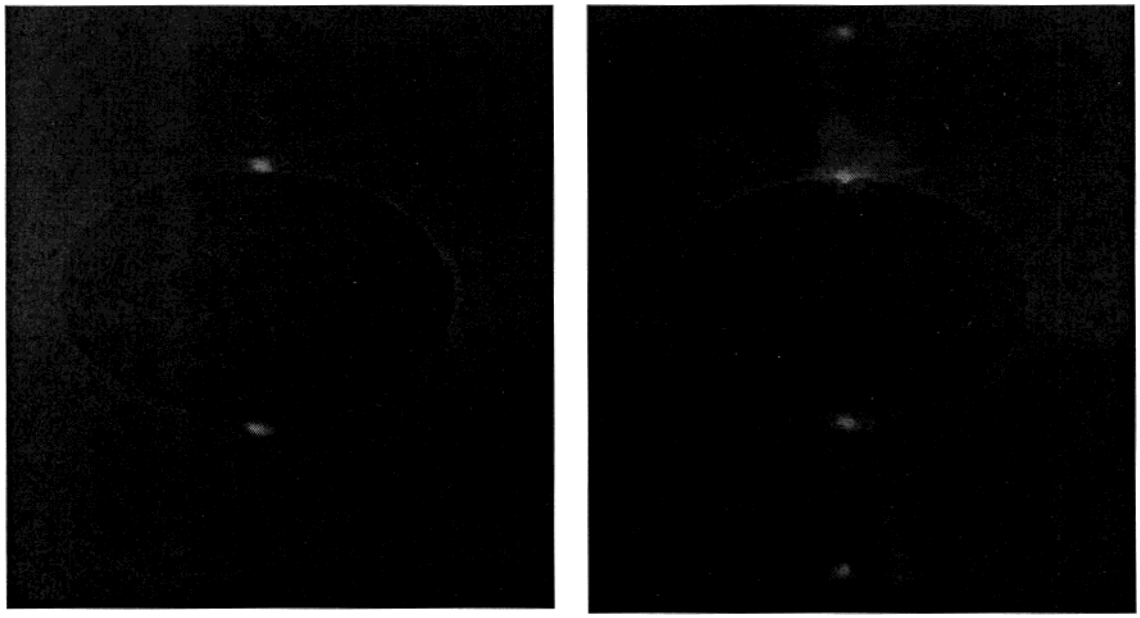

Figure 5. Diffraction patterns from the 2 min radiation sample and 6 min radiation sample under 2-D light scattering device.

displaying higher-order diffraction peaks. The emergence of second- or higher-order peaks is the manifestation of interface sharpening associated with the transformation of the sinusoidal concentration profile to nonsinusoidal profiles in the bulk such as cosine square-wave or truncated flat-top types, although it will be difficult to distinguish the detailed topologies among the nonsinusoidal patterns.

In order to gain further insight into the above experimental observations, a numerical simulation was carried out in the context of the reaction−diffusion model discussed in the theoretical section. Figure 6 (left column) illustrates the spatiotemporal evolution of microchannel layer patterns emerging from two-wave interference, calculated under the conditions $N_x = 8$ and $k = 10^{-4}$. For convenience, the structure development will be analyzed in terms of polymer concentration since the monomer and polymer concentrations are interdependent variables, i.e., $\phi_m + \phi_p = 1$, disregarding the possible volume shrinkage during polymerization.

Initially the reaction was triggered by perturbation of thermal noise, and it was removed in subsequent runs. At the onset of reaction, $\phi_p(r,t)$ was computed for each r and t under the periodic boundary conditions. It is apparent that the stratified patterns reveal no internal structure within each dark and bright channel, indicative of a single-phase character. The dark channels in the polymer concentration field refer to the polymer lean region where the intensity is low as a consequence of destructive interference, while the bright channels in the polymer concentration field refer to the polymer-rich region where the light intensity is high due to the constructive interference. It also can be noticed that the bright channels in the polymer concentration field expand in the vertical direction, implying a broadening of the emerging polymer network.

The length scale of the microchannel layer can be estimated via the relationship $\tau = (D_m/l^2)\tau$ and $\kappa = (l^2/D_m)\kappa$. Note that τ and κ are dimensionless time and reaction constant used in the simulation, and D_m is the diffusion coefficient of monomer. Once the data of the experimental time and diffusion coefficient become available, one can estimate the characteristic length l and approximate the width of each channel layer as well as the periodic distance thereof.

In our case, the diffusion coefficient of acrylic monomer is around 10^{-11} cm^2/s within the reported range,[22] the experimental exposure time is about 10^3 s, and the simulated time is nearly 10^4 time steps. Thus, the characteristic length l is approximately 100 nm, and the width of the microchannel layer in our case is around $1-3$ μm.

The right column in Figure 6 is the Fourier transform of the morphology pattern on the left. A gradual evolution from dual diffraction peaks to higher orders was evident from 1000 to 20 000 time steps. This is remarkably consistent with the experimental findings in the previous figures.

For the purpose of better visualizing the patterns, we present a vertical slice of the microchannel layer of Figure 6. Because of the symmetry, only a quarter of the polymer concentration is shown in Figure 7 for various time steps. In Figure 7, one can discern the sinusoidal variation of the polymer concentration for some initial periods. However, with the progression of the reaction, the peaks, corresponding to the polymer network region, tend to broaden, which is consistent with what was observed experimentally (Figure 6). Of particular interest is the transformation of polymer concentration profile from initially sinusoidal to various truncated wave forms. That is to say, with the progression of reaction time, the sinusoidal peaks level off, and then gradually get truncated by flattening the top. A concave profile subsequently develops on the top of the truncated profile. A similar profile transition has been revealed by some other groups,[21,22] but no explanation was offered on its transformation. It is believed that the understanding of such structural change is crucial in regards to the fabrication of electrical-optical materials.

It may be speculated that the transition of such a sinusoidal to a truncated wave behavior is influenced by the competition between reaction kinetics and diffusion. At the onset of photopolymerization, the reaction kinetics tend to make the polymer concentration field sinusoidal, arising from the spatially modulated light intensity while the monomer diffusion tries to keep the

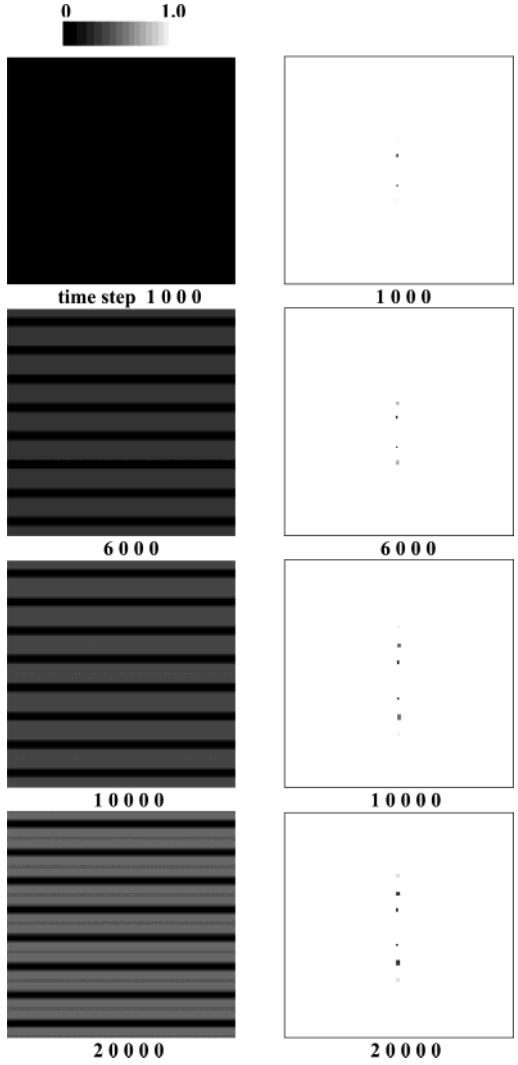

Figure 6. Spatial temporal evolution of morphology in polymer concentration field showing microchannel layer patterns (left column) and Fourier transform patterns of the corresponding morphology (right column).

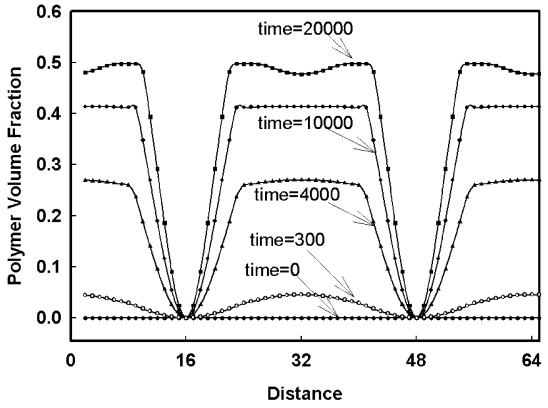

Figure 7. Profiles of emerging polymer volume fraction vs distance at various time steps from a vertical slice of the microchannel layer patterns, $k = 0.0001$.

monomer concentration field uniform. In the early time steps, the rate of conversion is large, and the reaction kinetics dominates such that the profiles of emerging polymer appear sinusoidal. In the intermediate to late time steps, the reaction kinetics slow, and thus diffusion becomes dominant. It can be noticed in the polymer concentration field that the reaction occurs predominantly at the interface. As monomers are pulled into the high-intensity region, those monomers are reacted at the interface close to the high-intensity region before these monomers can reach the interior region. Thus, the polymer concentration at the high-intensity region increases preferentially at the edges of the interface, while the low-intensity region shrinks due to the monomer depletion. As a consequence, the interface gradient becomes steeper. Since monomer molecules can hardly reach the bulk polymer region due to the fast reaction at the interface, the concentration profile of the polymer-rich region increasingly becomes truncated with time. Such an observation is believed to occur, especially when the intensity of the laser irradiation is sufficiently high.

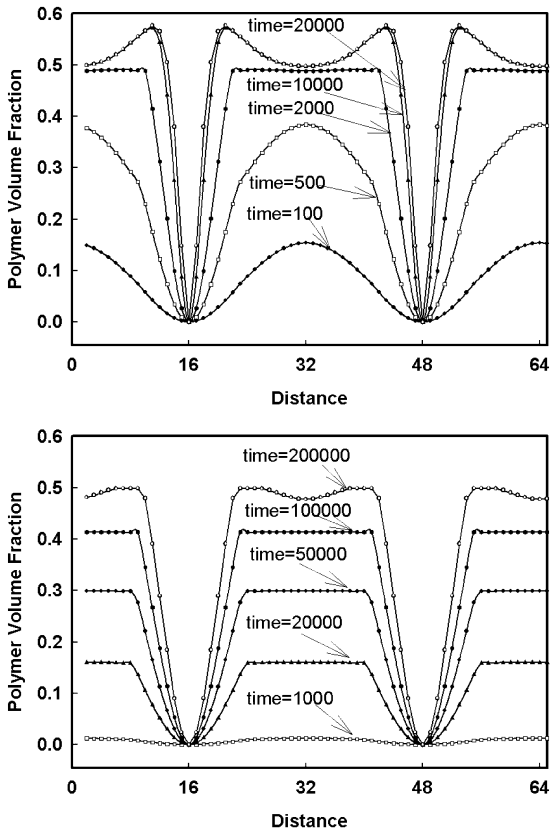

Figure 8. Profiles of emerging polymer volume fraction vs distance at various time steps from a vertical slice of the microchannel layer patterns at different reaction kinetic constant $k = 0.001$ (upper) and $k = 0.000\,01$ (lower).

To further check the effect of reaction kinetic constant on temporal evolution of the profile, we carried out two more simulations keeping all the parameters unchanged, except k. As can be seen in the upper row of Figure 8, the above-mentioned characteristics in Figure 7 are mostly reproducible in the calculation using $k = 0.001$. The only difference is that the truncation of the sinusoidal wave occurs earlier than the aforesaid case (i.e., time steps between 100 and 500), while in the lower row ($k = 0.000\,01$), the departure from the sinusoidal curve is slower than the previous case (i.e., time steps around 1000 and 20 000). It should be emphasized from Figure 8 that the enhanced light intensity accelerates the dynamics of pattern photopolymerization-induced transport; however, it does not seem to create any new profiles. This suggests that the transition from the sinusoidal to the truncated profiles becomes independent of the reaction kinetic constant, gradually reaching the asymptotic dynamic behavior.

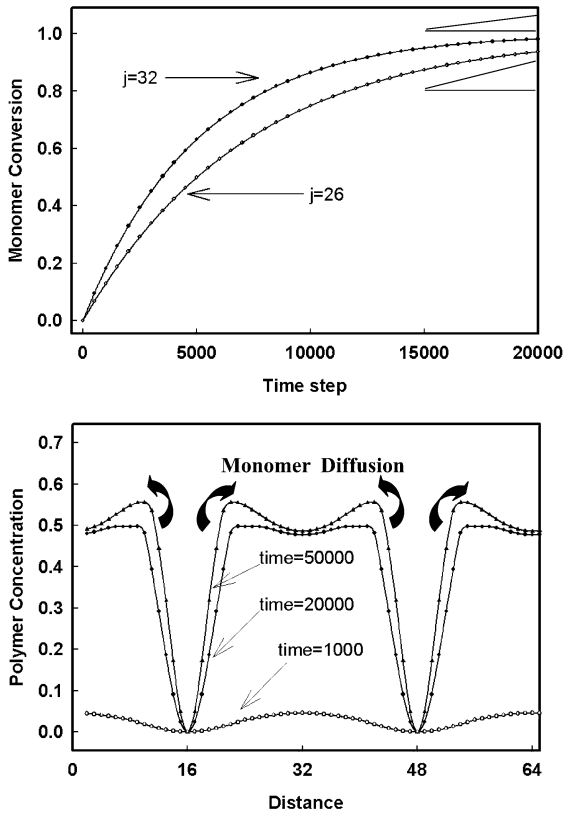

Figure 9. Polymer conversion vs time steps at various position ($j = 26$, 32) of vertical slice (upper) and illustrative demonstration of monomer diffusion in the interface of microchannel layer patterns, $k = 0.0001$ (lower).

Furthermore, it should be emphasized that the reaction kinetic constant used in the simulations is actually a complicated function of light intensity, photoreaction involving initiation, propagation, termination rate, monomer concentration, monomer functionality, self-diffusion coefficient, etc. More inputs, both quantitative modeling and experiments, need to be investigated in this area.

To improve further understanding on the transition of sinusoidal to nonsinusoidal profiles, we plot the monomer conversion vs time steps at two different locations ($j = 26$, 32) on the vertical slice direction in Figure 9 (upper row). Here $j = 32$ corresponds to the highest light intensity site, whereas $j = 26$ is a spot close to the edge of the interface. Between the time steps from 15 000 to 20 000, it was found that the slope of at the edge ($j = 26$) is higher than that of the bulk ($j = 32$), which in turn implies that the rate of monomer conversion in the highest intensity region is lower than that at the interface. Presumably more monomers diffuse into the interface and get reacted before they can reach the highest intensity region, as illustrated in the bottom row of Figure 9. Consequently, the stack of emerging polymer at the interface creates a conspicuous concave shape between 20 000 and 50 000 time steps.

Summary

Photopolymerization-induced transport patterning process was simulated by incorporating the simple diffusion equation coupled with reaction kinetic equation. The transition from the sinusoidal concentration profiles to the truncated flat-top profiles and then to the concave-top profile was predicted theoretically. The predicted nonsinusoidal waves may be a consequence that the monomer molecules are presumably pulled into the high-intensity region of the emerging polymer network by climbing along the interface. However, by virtue of the fast photoreaction triggered by the strong laser light source, these molecules get reacted before they can reach the highest intensity region. This behavior manifests the complex photoreaction in the pattern polymerization. Finally, the microlayer pattern was produced experimentally and characterized by OM and AFM. The close examination of the 2-D diffraction patterns as a function of radiation time revealed an evolution of higher-order diffraction peaks, implying the transformation from sinusoidal to nonsinusoidal waves in the bulk, which was quite consistent with the theoretical predictions.

Acknowledgment. The UA group acknowledged the support from the National Science Foundation through Grant DMR 02-09272 and the Ohio Board of Regents Research Challenge Grant. The collaboration was made possible through the support of the Polymer Photonic Collaborative Center (CCPP), sponsored by University of Akron, Air Force Office of Scientific Research, and Materials and Manufacturing Directorate, Wright-Patterson Air Force.

References and Notes

(1) Scranton, A. B.; Bowman, C. N.; Peiffer, R. W. *ACS Symp. Ser.* **1997**, *673*, 16.
(2) Sutherland, R. L.; Tondiglia, V. P.; Natarajan, L. V.; Bunning, T. J. *Appl. Phys. Lett.* **2001**, *79*, 1420.
(3) Sutherland, R. L.; Tondiglia, V. P.; Natarajan, L. V.; Bunning, T. J.; Adams, W. W. *Appl. Phys. Lett.* **1994**, *64*, 1074.
(4) Kyu, T.; Nwabunma, D. *Macromolecules* **2001**, *34*, 9168.
(5) Wang, X. Y.; Yu, Y. K.; Taylor, P. L. *J. Appl. Phys.* **1996**, *80*, 3285.
(6) Kyu, T.; Nwabunma, D.; Chiu, H. W. *Phys. Rev. E* **2001**, *63*, 1802.
(7) Caputo, R.; Sukhov, A. V.; Tabirian, N. V.; Umeton, C.; Ushakov, R. F. *Chem. Phys.* **2001**, *271*, 323.
(8) Mitrofanov, A. V. *J. Moscow Phys. Soc.* **1999**, *9*, 147.
(9) Meng, S.; Nwabunma, D.; Kyu, T. *Mater. Res. Soc. Symp. Proc. Ser.* **2002**, *709*, 197.
(10) Schnoes, M. G.; Dhar, L.; Schilling, M. L.; Patel, S. S.; Wiltzius, P. *Opt. Lett.* **1999**, *24*, 658.
(11) Ilavsky, M.; Bonchal, K.; Dusek, K. *Makromol. Chem.* **1989**, *190*, 883.
(12) Cahn, J. W.; Hilliard, J. E. *J. Chem. Phys.* **1958**, *28*, 258.
(13) Chiu, H. W.; Kyu, T. *J. Chem. Phys.* **1999**, *110*, 5998.
(14) Stanley, H. E. *Introduction to Phase Transitions and Critical Phenomena*; Oxford University Press: New York, 1971.
(15) de Gennes, P. G. *J. Chem. Phys.* **1980**, *72*, 4756.
(16) Gunton, J. D.; San Miguel, M.; Sahni, P. S. *Phase Transitions and Critical Phenomena*; Academic Press: New York, 1983.
(17) Atkins, P. W. *Physical Chemistry*, 5th ed.; W.H. Freeman and Co.: New York, 1994.
(18) Nwabunma, D.; Chiu, H. W.; Kyu, T. *J. Chem. Phys.* **2000**, *113*, 6429.
(19) Odian, G. *Principles of Polymerization*, 2nd ed.; Wiley-Interscience: New York, 1981.
(20) Zhao, G.; Mouroulis, P. *J. Mod. Opt.* **1994**, *41*, 1929.
(21) Colvin, V. L.; Larson, R. G.; Harris, A. L.; Schilling, M. L. *J. Appl. Phys.* **1997**, *81*, 5913.
(22) Bowley, C. C.; Crawford, G. P. *Appl. Phys. Lett.* **2000**, *76*, 2335.

MA0356055